Complex dynamic behaviour of methanol synthesis in the ring reactor network

This is the author's copy of the paper:

Velardi S., Barresi A. A., Manca D., Fissore D. (2004). Complex dynamic behaviour of methanol synthesis in the ring reactor network. Chemical Engineering Journal (Elsevier), 99(2), 117-123. DOI: 10.1016/j.cej.2003.09.008.

Complex Dynamic Behaviour of Methanol Synthesis in the Ring Reactor Network

by Salvatore VELARDI[1], Antonello A. BARRESI[1*], Davide MANCA[2] and Davide FISSORE[1]

[1]Politecnico di Torino, Dipartimento di Scienza dei Materiali ed Ingegneria Chimica, Corso Duca degli Abruzzi 24, 10129 Torino, Italy.
Tel. +39-011-5644658, Fax: +39-011-5644699, E-mail: antonello.barresi@polito.it.

[2]Politecnico di Milano, Dipartimento di Chimica, Materiali e Ingegneria Chimica, Piazza Leonardo da Vinci 32, 20133 Milano Italy
Tel. +39-02-23993271, Fax: +39-02-70638173, E-mail: davide.manca@polimi.it

[*] Author to whom all the correspondence should be addressed

Abstract

The dynamic behaviour of a three reactors network (or ring reactor), with periodic change of the feed position, has been investigated in a previous work for low pressure methanol synthesis, showing that cyclic steady states and autothermal processing can be obtained, leading to higher conversions than traditional devices. Furthermore, complex dynamics - highly periodic steady states and multiplicity of periodic steady states - may arise, close to the conditions of maximum conversion. A simple open loop control policy, which can be useful for a safe start-up, has been also tested to study the response of the network to disturbances on the input parameters, showing that a more robust control strategy is needed for this application.

Keywords

Forced unsteady-state reactors, equilibrium-limited reactions, methanol synthesis, complex dynamic, open loop control.

1. Introduction

Forced unsteady-state catalytic reactors have received much attention in recent years, as concerns both industrial applications and scientific investigation and have been proposed both for endothermal and exothermal processes as well as for reversible and equilibrium reactions. Favourable temperature and composition distributions, which cannot be attained in any steady-state regime, can be reached by means of forced variations of inlet parameters, as it has been showed in [1]. The periodic reversal of the flow direction is a simple technical solution to obtain forced unsteady-state conditions. Extensive investigations about the reverse-flow reactor have been performed in the past thirty years (see the review works [2, 3]), showing that this device can be used for the combustion of lean and cold mixtures as the reversal of the flow keeps the heat of reaction inside the bed, which acts as a regenerative heat exchanger, thus reducing the need for auxiliary fuel, except for start-up [1, 4]. Another advantage of this configuration is the possibility to achieve an optimal temperature distribution, which makes possible the creation of favourable thermodynamic conditions for exothermic equilibrium-limited reactions.

The ring reactor, or reactor network, consists of a sequence of two or more catalytic fixed bed reactors in which a sustained dynamic behaviour is obtained through the periodical variation of the feed position. In this work we consider a network made of three reactors, as shown in Figure 1: the sequence of the reactors is changed after a time t_c, acting on a set of valves. By this way, contrary to the reverse-flow reactor, the flow direction is maintained ensuring a uniform catalyst exploitation.

This reactor configuration has received little attention up to now. A comparison between the reverse-flow reactor and a network of two reactors is given in [5], pointing out that in the network there is only a small range of switching times in which stable operation can be obtained. A sequence of three beds was investigated in [6, 7] to demonstrate the feasibility of this solution for the combustion of lean VOC emissions. Preliminary results confirmed that this device can be competitive, in certain conditions, with the reverse-flow combustor, as it strongly reduces the emissions of unburned gas due to wash-out, in correspondence of each switch. Autothermal behaviour can be obtained, even at low VOC concentration, but safe operation is limited to a narrow

range of switching times. Consequently, a more robust control policy than the open loop strategy, based on fixed switching times, has been proposed [7, 8]. The influence of the number of reactors in the network and of the main operating parameters on the performance of the device has been recently investigated [9].

In the case of exothermic, equilibrium-limited synthesis reactions the aim is to approach the ideal profile of maximum product generation. The feasibility of synthesis gas production by means of catalytic partial oxidation of methane in a network of three reactors and the influence of the main operating parameters has been demonstrated in [10], showing that conversion and selectivity are similar to those that can be obtained in a reverse-flow reactor. In this work methanol synthesis will be considered, as it was shown in [11] that this process, when carried out in a reverse-flow reactor, can give higher conversion in comparison to traditional steady-state technology, based on multi-bed adiabatic reactors. Velardi and Barresi have demonstrated the feasibility of this process in a three reactors network [12], showing that in certain conditions higher conversion and selectivity can be obtained in comparison to traditional technologies. In this work the influence of the main operating parameters on the dynamic behaviour of this configuration operated with an open loop control strategy has been studied, with particular attention to the possibility of highly periodic steady-states. Furthermore the dynamic response of the system to external disturbances has been considered.

2. Model

A one-dimensional heterogeneous model has been adopted for the numerical simulations. A network of three adiabatic reactors has been considered, with plug flow condition for the gas phase. Mass and energy dispersive transport have been taken into account as well as the transient terms in the gas phase equations and in the energy equation for the solid. The time-dependent term in the mass balance for the solid phase has been neglected, thus leading to a pseudo-steady-state condition for the catalyst surface. The set of algebraic-differential equations that describes the dynamics of the system is the following:

- Continuity equation for the gas phase:

$$\frac{\partial c_G}{\partial t} + \frac{\partial}{\partial x} c_G v = \sum_{i=1}^{n_r} \frac{k_{G,i} a_v}{\varepsilon} (y_{S,i} - y_{G,i}) \tag{1}$$

- Continuity equation for component *j* in the gas phase:

$$\frac{\partial y_{G,j}}{\partial t} = D_{eff} \frac{\partial^2 y_{G,j}}{\partial x^2} - v \frac{\partial y_{G,j}}{\partial x} + \frac{k_{G,j} a_v}{c_G \varepsilon} \left(y_{S,j} - y_{G,j} \right) - y_{G,j} \sum_{i=1}^{n_r} \frac{k_{G,i} a_v}{c_G \varepsilon} \left(y_{S,i} - y_{G,i} \right) \tag{2}$$

with $j = 1 \ldots (n_r - 1)$

- Energy balance for the gas phase:

$$\frac{\partial T_G}{\partial t} = \frac{k_{eff}}{\varrho \hat{c}_{P,G}} \frac{\partial^2 T_G}{\partial x^2} - v \frac{\partial T_G}{\partial x} + \frac{h a_v}{\varrho \hat{c}_{P,G} \varepsilon} (T_S - T_G) \tag{3}$$

- Mass balance for the solid phase:

$$k_{G,j} a_v \left(y_{S,j} - y_{G,j} \right) = \left[\varrho_S (1 - \varepsilon) \right] \sum_{k=1}^{N_R} \eta_k \nu_{j,k} R_k' \quad \text{with} \quad j = 1 \ldots n_r \tag{4}$$

- Energy balance for the solid phase:

$$\frac{\partial T_S}{\partial t} = \frac{\lambda_S}{\varrho_S \hat{c}_{P,S}} \frac{\partial^2 T_S}{\partial x^2} - \frac{h a_v}{\varrho_S \hat{c}_{P,S} (1 - \varepsilon)} (T_S - T_G) + \frac{1}{\hat{c}_{P,S}} \sum_{i=1}^{n_r} \left(\sum_{k=1}^{N_R} \eta_k \nu_{i,k} R_k' \right) (-\Delta \tilde{H}_{f,i}) \tag{5}$$

The model is completed by the kinetic equations by Graaf et al. [14], corresponding to a dual-site Langmuir-Hinshelwood mechanism, based on three independent reactions: methanol formation from CO, water-gas-shift reaction and methanol formation from $\mathrm{CO_2}$:

(A) $\mathrm{CO} + 2\mathrm{H_2} \rightleftharpoons \mathrm{CH_3OH}$ (6)

(B) $\mathrm{CO_2} + \mathrm{H_2} \rightleftharpoons \mathrm{CO} + \mathrm{H_2O}$ (7)

(C) $\mathrm{CO_2} + 3\mathrm{H_2} \rightleftharpoons \mathrm{CH_3OH} + \mathrm{H_2O}$ (8)

The reaction rates for methanol and water from reactions (A), (B) and (C) are given by the following equations, according to Graaf et al. [14]:

$$R'_{\mathrm{CH_3OH,\,A}} = \frac{k'_{\mathrm{ps,A}} K_{\mathrm{CO}} \left[p_{\mathrm{CO}} p_{\mathrm{H_2}}^{3/2} - p_{\mathrm{CH_3OH}} \Big/ \left(p_{\mathrm{H_2}}^{1/2} K_{p,\mathrm{A}} \right) \right]}{\left(1 + K_{\mathrm{CO}} p_{\mathrm{CO}} + K_{\mathrm{CO_2}} p_{\mathrm{CO_2}} \right) \left[p_{\mathrm{H_2}}^{1/2} + \left(K_{\mathrm{H_2O}} \Big/ K_{\mathrm{H_2}}^{1/2} \right) p_{\mathrm{H_2O}} \right]} \tag{9}$$

$$R'_{\mathrm{H_2O,\,B}} = \frac{k'_{\mathrm{ps,B}} K_{\mathrm{CO_2}} \left(p_{\mathrm{CO_2}} p_{\mathrm{H_2}} - p_{\mathrm{H_2O}} p_{\mathrm{CO}} \Big/ K_{p,\mathrm{B}} \right)}{\left(1 + K_{\mathrm{CO}} p_{\mathrm{CO}} + K_{\mathrm{CO_2}} p_{\mathrm{CO_2}} \right) \left[p_{\mathrm{H_2}}^{1/2} + \left(K_{\mathrm{H_2O}} \Big/ K_{\mathrm{H_2}}^{1/2} \right) p_{\mathrm{H_2O}} \right]} \tag{10}$$

$$R'_{\mathrm{CH_3OH,\,C}} = R'_{\mathrm{H_2O,\,C}} = \frac{k'_{\mathrm{ps,C}} K_{\mathrm{CO_2}} \left[p_{\mathrm{CO_2}} p_{\mathrm{H_2}}^{3/2} - p_{\mathrm{CH_3OH}} p_{\mathrm{H_2O}} \Big/ \left(p_{\mathrm{H_2}}^{3/2} K_{p,\mathrm{C}} \right) \right]}{\left(1 + K_{\mathrm{CO}} p_{\mathrm{CO}} + K_{\mathrm{CO_2}} p_{\mathrm{CO_2}} \right) \left[p_{\mathrm{H_2}}^{1/2} + \left(K_{\mathrm{H_2O}} \Big/ K_{\mathrm{H_2}}^{1/2} \right) p_{\mathrm{H_2O}} \right]} \tag{11}$$

Concerning the gas-solid heat transfer coefficient, the following correlation has been adopted:

$$\frac{h d_{\mathrm{P}}}{\lambda_G} = 1.6 \left(2 + F \cdot \mathrm{Re_P^{0.5}} \, \mathrm{Pr^{1/3}} \right) \tag{12}$$

with

$$F = 0.664 \sqrt{1 + \left[\frac{0.0557 \cdot \mathrm{Re_P^{0,3}} \, \mathrm{Pr^{2/3}}}{1 + 2.44 \left(\mathrm{Pr^{2/3}} - 1 \right) \mathrm{Re_P^{-0,1}}} \right]^2} \tag{13}$$

and a similar correlation has been considered for the mass transfer coefficient, according to Chilton-Colburn's analogy (see [6] for further details).

The prediction of the axial heat dispersion coefficient has been carried out adopting a correlation by Dixon and Cresswell [15]:

$$\frac{k_{eff}}{\varrho v \hat{c}_{\mathrm{P,G}} d_{\mathrm{P}}} = \frac{0.73 + \lambda_{st} / \lambda_G}{\mathrm{Re_P \, Pr}} + \frac{0.5}{1 + 9.7 / \left(\mathrm{Re_P \, Pr} \right)} \tag{14}$$

where the term λ_{st} / λ_G represents the stagnant zone contribution. According to Edwards and Richardson [16] a correlation of the same general form as the (14) can be used for the prediction of mass dispersion coefficient:

$$\frac{D_{eff}}{v d_{\mathrm{P}}} = \frac{0.73}{\mathrm{Re_P \, Sc}} + \frac{0.5}{1 + 9.7 / \left(\mathrm{Re_P \, Sc} \right)} \tag{15}$$

The effectiveness factors η_k in equation (4) have been estimated following the linearization procedure described in [13].

Conventional Danckwerts boundary conditions are assumed at the inlet section of the network. The continuity of the gas temperature and concentration profiles has been imposed between each reactor of the sequence, at sections $x = l$ and $x = 2l$. In addition, spatial derivatives should vanish at the outlet sections. At time $t = 0$ the reactants concentration is null, while the initial temperatures of the gas and solid phases are the same. When the switching time is reached the origin of the x-axis moves from the first reactor of the sequence to the second one and the switching conditions are applied in order to simulate the change of the inlet position:

$$x \in]0, 2\ell[\qquad \begin{cases} y_{G,j}(x)\big|_{t^+} = y_{G,j}(x+\ell)\big|_{t^-} \\ T_G(x)\big|_{t^+} = T_G(x+\ell)\big|_{t^-} \\ T_S(x)\big|_{t^+} = T_S(x+\ell)\big|_{t^-} \end{cases} \tag{6}$$

$$x \in [2\ell, 3\ell] \qquad \begin{cases} y_{G,j}(x)\big|_{t^+} = y_{G,j}(x-2\ell)\big|_{t^-} \\ T_G(x)\big|_{t^+} = T_G(x-2\ell)\big|_{t^-} \\ T_S(x)\big|_{t^+} = T_S(x-2\ell)\big|_{t^-} \end{cases}$$

The domain of the spatial variable x has been discretised on a grid of equally spaced points; 101 points are sufficient to ensure a grid-independent solution. As a consequence, the partial differential algebraic equations system (PDAE) (1)-(6) is transformed into a differential algebraic equations (DAE) problem: the algebraic system of non linear equations resulting from the mass balance on the solid has been solved through the routine BUNSLI [17], while the integration in time of the differential part of the system has been performed implementing the Fortran routine LSODES, from the package ODEPACK [18]. Both relative and absolute tolerance are set to the square root of the working machine precision. The parameter values used in simulations are given in Table 1, and correspond to the conditions adopted in a previous work on the reverse flow operation of methanol synthesis [19].

After a transient period, the solution of the system evolves towards a periodic-steady state: the behaviour of the reactor (temperature and concentration profiles) is the same within every three switches.

3. Results

3.1 Operating ranges

Figure 2 shows the performance of the network of three reactors for different values of the switching time. Numerical simulations reveal that the network can operate in two regions of t_c values: the high t_c and the low t_c operating range, separated by a region in which extinction occurs. Autothermal behaviour is possible because no energy supply is needed, except a moderate preheating of the feeding, required to avoid the condensation of the reactants. Nevertheless, the solid bed must be preheated above the ignition temperature in order to prevent extinction during start-up and to attain autothermal processing. Therefore, an initial temperature of the bed T_S^0 = 220°C was chosen for simulations in the high t_c range, while a value of T_S^0 = 290°C was required in order to have a safe start-up at low t_c values.

When the switching frequency is high the heat and mass transfer evaluated according to eq.(12) may not be adequate to describe the transport process as the correlation has been proposed for steady-state conditions, which are not obtained when t_c is low. As it is extremely difficult to have reliable estimations of the heat and mass transfer coefficients in these conditions, the sensitivity of the model to these parameters has been evaluated, by changing the value of the heat transfer coefficient (and also the mass transfer coefficient according to Chilton-Colburn's analogy). Figure 2 shows the carbon to methanol conversion when these coefficients are 5 and 10 times higher than in the base case (eq. 14): the range of t_c in which the operation is feasible is the same, even if the conversion slightly decreases whene the value of the coefficients is increased; if the heat and mass transfer coefficients are further increased, no further decrease in the conversion is noticed, as when they are reduced with respect to the base case. The same analysis has been repeated in the high t_c range, leading to analogous results: the value of the heat and mass trasfer coefficient slightly affects the carbon to methanol conversion, but it does not affect the dynamic behaviour and the range of t_c where stable oepration can be obtained. As a consequence, in the followings, the values of heat and mass transfer coefficients are evaluated according to eq. (12).

Figure 3 shows a comparison between typical temperature and conversion profiles in the two operating ranges. At high t_c (dashed lines) profiles are very similar to those obtainable in a reverse flow reactor. Initially, the positive slope of the temperature wave brings the fresh feed above the ignition temperature (≈ 180°C) so that the exothermic synthesis reaction starts with heat generation. In correspondence of the maximum temperature an equilibrium plateau is approached by the conversion profile. When the temperature decreases at the downstream end of the wave, conversion increases because methanol synthesis equilibrium is shifted towards higher values. Finally, when the temperature falls below the ignition value, the reaction rate becomes negligible and a second plateau is observed. At low t_c values (Figure 3, continuous lines) the switching strategy implemented in the reactor network leads to the formation of profiles that present a series of temperature drops. These are somewhat analogous to intermediate coolings, which shift the reaction far from equilibrium, thus allowing the conversion to continuously increase along the beds. Since this effect becomes more important as the switching time increases, methanol conversion enhances with t_c while operating in the low t_c range, as it is shown in Figure 2. As we increase the switching time, working at high t_c values, the hot central section of the network enlarges, while the downstream end of the temperature wave tends to leave the system. Consequently, the increment in conversion, given by the final temperature reduction, becomes smaller. This results in the decrease of methanol conversion *vs* the switching time in the high t_c range, which is showed in Figure 2.

3.2 Complex behaviour region

If the switching time belongs to the high t_c operating range, transition from stable periodic operation to a non-ignited state occurs at a precise value of t_c; while operating at low switching time, transition to extinction is not well defined, but it takes place through a region where highly periodic solutions are obtained with lower conversion. Even if permanent pseudo-steady-state conditions have been reached, the profiles in a generic cycle are different from the others since the material and energy balances have a solution of period greater than the cycle time. For example, Figure 4 shows the temperature and concentration profiles in three subsequent cycles for a switching time of 20 s.

An example of high periodicity of the solution is shown in Figure 5, where, for t_c = 20 s, the evolution of the average methanol conversion is plotted vs. the number of operating cycles. If we choose two representative variables (e.g. outlet gas temperature and methanol conversion) the status of the reactor during a cycle can be defined by a unique couple of values, both operating in the high and in the low switching time range. Conversely, in the complex behaviour region, the status of the system can be represented by a stroboscopic map, given by a number of points equal to the number of cycles corresponding to the periodicity of the solution. The stroboscopic map of Figure 6 (left hand side) shows that 47 combinations of outlet gas temperature and methanol conversion are possible when t_c = 20 s, each one corresponding to one of the 47 cycles of the period. If we change t_c also the period of the solution changes. As we move away from the stability operation range the period of the solution increases up to a value of 332 t_c (right hand side), which corresponds to the upper limit of this high periodicity range.

3.3 Open loop response to disturbances

Numerical simulations reveal that high conversion can be obtained in a network of three reactors operating in unsteady-state conditions, but care must be paid to the existence of unstable regions of operation, which separate stable zones where profile along the reactor are completely different. In order to attain and maintain stable periodic operations a simple open-loop control strategy was adopted, which consists of the periodic alternations of the inlet sections at fixed time interval t_c. The knowledge of the dynamic behaviour of the reactor is quite important for the control of such a system, because the condition of maximum yield is very close to the zones of complex periodic behaviour. Furthermore, the useful operating ranges have a narrow extension, so even small disturbances may drive the reactor out of optimum. For example, for a -10°C step disturbance in the inlet temperature the reactor falls outside the operating range at low t_c values. The slow transition to a complex periodic steady-state can be observed in Figure 7. The system exhibits an inverse response, because initially the average carbon to methanol conversion oscillates around 0.59, which improves of about 5% the performance of the optimal network configuration. Nevertheless, the oscillations become larger and the outlet conversion falls down after 150 switches from the

disturbance. Finally, a pseudo-steady condition is approached, in which a solution of 48 t_c is obtained.

If the disturbance has a relatively short length and the switching time is not changed, the system is able to take the average conversion back to its original value. This is shown in Figure 8, which shows the evolution of the mean conversion when the disturbance of -10°C on the inlet temperature stops after 195 cycles, before the new cyclic steady-state has been reached. After a long time disturbance the system is not able to return to the original state without changing the switching time. Figure 9 shows the performance of the network when the disturbance $\Delta T_{G,\,in}$ = -10°C stops after 200 cycles. It can be seen that the reactor does not return to the optimal conditions, but it falls in a new highly periodic steady-state, thus outlining the existence of multiple periodic steady states.

As a consequence of these results, a control scheme for this device has to face any disturbances both in the inlet temperature and in the flow rate, as also when the inlet velocity changes the reactor may exhibit similar complex behaviours. This may be accomplished for example by any commercial PID controller. If a tighter control on the outlet methanol conversion is needed a model predictive control (MPC) scheme should be used, varying the switching time to maximise the selectivity of the reactor; the on-line optimisation requires the use of a simplified model and this will be the subject of a future work.

4. Conclusions

The dynamic behaviour of a network of three catalytic fixed bed reactors, with periodical variation of the feed position, has been investigated by means of numerical simulations. The mildly exotermic, equilibrium-limited methanol synthesis process has been considered. A cyclic unsteady state regime with autothermal behaviour can be reached in such a reactor, but this is achievable only for switching times varying in two distinct ranges: the high t_c and the low t_c operating regions. Out of the useful operating regions, two other reactor states are possible: extinction or complex behaviour. In the latter, cyclic steady states of period greater than the switching time are observed, in which poor performances are expected. It has been shown that in this complex

behaviour region, the periodicity of the solutions increases as the limit of extinction is approached.

The achievement of a sustained cyclic regime is made possible by an open loop control strategy, which consists of the periodic switching of the feed at a fixed time interval t_c. This open-loop control allows for a safe start-up, with an appropriate choice of the bed pre-heating temperature, but it can be ineffective if the inlet conditions are subject to fluctuations. Furthermore, the simulations of the response of the system to disturbances pointed out the existence of multiple highly periodic steady states close to the optimum zone. As a consequence, more robust control strategies must be adopted.

Acknowledgements

This work has been financially supported by Politecnico of Torino (Young Researchers Project).

Notation

a_v	external particle surface area per unit volume of reactor, m^{-1}
c	molar concentration, $\mathrm{mol\ m}^{-3}$
$\hat{c}_P$	specific heat at constant pressure, $\mathrm{J\ kg}^{-1}\mathrm{K}^{-1}$
D_{eff}	effective mass dispersion coefficient, $\mathrm{m}^2\mathrm{s}^{-1}$
d_P	pellet diameter, m
F_{in}	superficial inlet flow rate, $\mathrm{mol\ m}^{-2}\mathrm{s}^{-1}$
$\Delta\tilde{H}_f$	molar enthalpy of formation, $\mathrm{J\ mol}^{-1}$
h	gas-solid heat transfer coefficient, $\mathrm{J\ m}^{-2}\mathrm{K}^{-1}\mathrm{s}^{-1}$
K	adsorption equilibrium constant, bar^{-1}
K_p	chemical equilibrium constant based on partial pressure
k_{eff}	effective heat dispersion coefficient, $\mathrm{J\ m}^{-1}\mathrm{K}^{-1}\mathrm{s}^{-1}$
k_G	gas-solid mass transfer coefficient, $\mathrm{mol\ m}^{-2}\mathrm{s}^{-1}$
k'_{ps}	reaction rate constant, mol s^{-1} kg^{-1} atm^{-1}
L	total network length, m
ℓ	single reactor length, m
N_R	number of reactions
n_r	number of components in the mixture
Pr	Prandtl number
R'	reaction rate, $\mathrm{mol\ s}^{-1}\mathrm{kg}^{-1}$
$\mathrm{Re_P}$	particle Reynolds number
Sc	Schmidt number
T	temperature, K
t	clock time, s
t_c	switching time, s
v	interstitial velocity, $\mathrm{m\ s}^{-1}$
x	axial reactor coordinate, m
y	molar fraction
$z_{\mathrm{CH_3OH}}$	carbon to methanol conversion

Greek letters

ε	void fraction of the catalytic bed
η_k	effectiveness factor for reaction *k*

λ	thermal conductivity, J $\mathrm{m^{-1}K^{-1}s^{-1}}$
ν	stoichiometric coefficient
ϱ	density, $\mathrm{kg\ m^{-3}}$

Subscripts and superscripts

A	indicates $\mathrm{CH_3OH}$ from CO reaction
B	indicates $\mathrm{CH_3OH}$ from $\mathrm{CO_2}$ reaction
C	indicates water-gas-shift reaction
G	gas phase
S	solid phase or solid surface
st	stagnant
in	inlet condition
0	initial condition

References

[1] Y. S. Matros, G. K. Bunimovich, Catal. Rev.-Sci. Eng. 38 (1996) 1.

[2] G. K. Boreskov, Y. S. Matros, Catal. Rev.-Sci. Eng. 25 (1983), 551.

[3] Y. S. Matros, Canad. J. Chem. Eng. 74 (1996) 566.

[4] G. Eigenberger, Fixed bed reactors, in: Ullmann's Encyclopedia of chemical industry, Vol. B4 VCH, Weinheim, 1992, pp. 199-238.

[5] T. N. Haynes, H. S. Caram, Chem. Eng. Sci. 49 (1994) 5465.

[6] M. Brinkmann, A. A. Barresi, M. Vanni, G. Baldi, Catal. Today 47 (1999) 263.

[7] A. A. Barresi, M. Vanni, M. Brinkmann, G. Baldi, AIChE J. 45 (1999) 1597.

[8] A. A. Barresi, M. Vanni, Dynamics and control of forced-unsteady-state catalytic combustors, in: Nonlinear dynamics and control in process engineering - Recent advances (G. Continillo, S. Crescitelli and M. Giona, Eds.), Springer-Verlag, Milano, 2002, pp. 73-88.

[9] D. Fissore, A. A. Barresi, Chem. Eng. Technol. 25 (2002) 421.

[10] D. Fissore, A. A. Barresi, G. Baldi, Ind. Eng. Chem. Res. 42 (2002) 2489.

[11] K. M. Vanden Bussche, G. F. Froment, Canad. J. Chem. Eng. 74 (1996) 729.

[12] S. Velardi, A. A. Barresi, Chem. Eng. Sci. 57 (2002) 2995.

[13] K. Gosiewski, U. Bartmann, M. Moszczynski, L. Mleczko, Chem. Eng. Sci. 54 (1999) 458.

[14] G. H. Graaf, E. J. Stamhuis, A. A. C. M. Beenackers, Chem. Eng. Sci. 43 (1988) 3185.

[15] A. Dixon, D. L. Cresswell, AIChE J., 25 (1979) 663.

[16] M. F. Edwards, J. F. Richardson, Chem. Eng. Sci., 23 (1968) 109.

[17] G. B. Ferraris, E. Tronconi, Comput. Chem. Eng. 10 (1986) 129.

[18] A. C. Hindmarsh, ODEPACK, a systematized collection of ODE solvers. Stepleman R. S. et al. Eds, Amsterdam, 1983.

[19] K. M. Vanden Bussche, S. N. Neophytides, I. A. Zolotarskii, G. F. Froment, Chem. Eng. Sci. 48 (1993) 3335.

Table 1. Parameters used in the numerical simulations

Total length	L	0.5	m
Void fraction	ε	0.4	
Catalyst density	ϱ_S	1750	kg m^{-3}
Catalyst specific heat	$\hat{c}_{P,S}$	1000	J kg^{-1} K^{-1}
Catalyst thermal conductivity	λ_S	0.33	W m^{-1} K^{-1}
Catalyst void fraction		0.5	
Pellet diameter	d_P	0.0054	m
Total pressure		5	MPa
Superficial inlet flow rate	F_{in}	32.65	mol m^{-2} s^{-1}
Feed composition			
CO		4.5	% mol
CO_2		2.0	% mol
CH_3OH		0.0	% mol
H_2O		0.0	% mol
H_2		93.5	% mol
Kinetic and equilibrium constants			
$k'_{ps,A}$	$2.69\cdot10^{7}\cdot\exp\left[-109900/\left(RT\right)\right]$		
$k'_{\mathrm{ps,B}}$	$7.31\cdot10^{8}\cdot\exp\left[-123400/\left(RT\right)\right]$		
$k'_{\mathrm{ps,C}}$	$4.36\cdot10^{2}\cdot\exp\left[-65200/\left(RT\right)\right]$		
K_{CO}	$7.99\cdot10^{-7}\cdot\exp\left[58100/\left(RT\right)\right]$		
$K_{\mathrm{CO_2}}$	$1.02\cdot10^{-7}\cdot\exp\left[67400/\left(RT\right)\right]$		
$K_{\mathrm{H_2O}}/K_{\mathrm{H_2}}^{1/2}$	$4.13\cdot10^{-11}\cdot\exp\left[104500/\left(RT\right)\right]$		
$\log_{10}K_{p,\mathrm{A}}$	$5139/T-12.621$		
$\log_{10}K_{p,\mathrm{B}}$	$-2073/T-2.029$		
$\log_{10}K_{p,\mathrm{C}}$	$3066/T-14.650$		

List of Figures

Figure 1

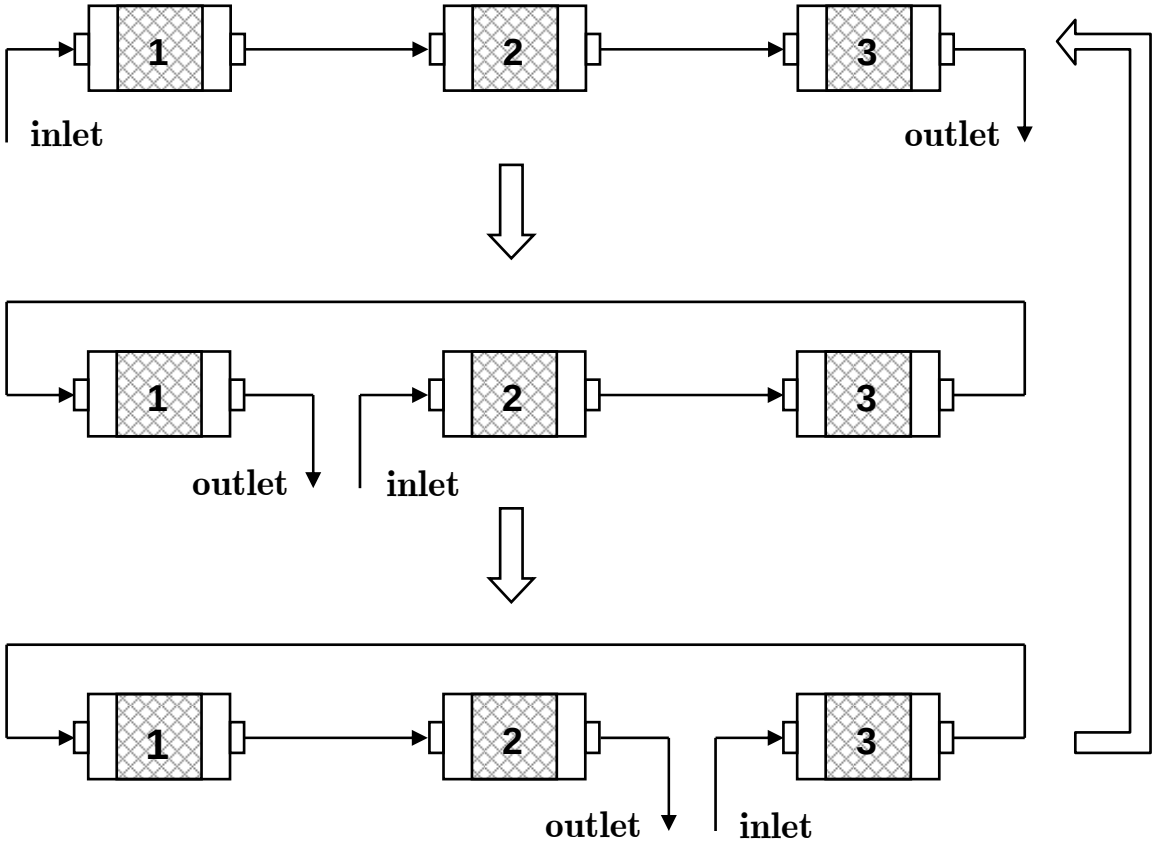

Figure 2

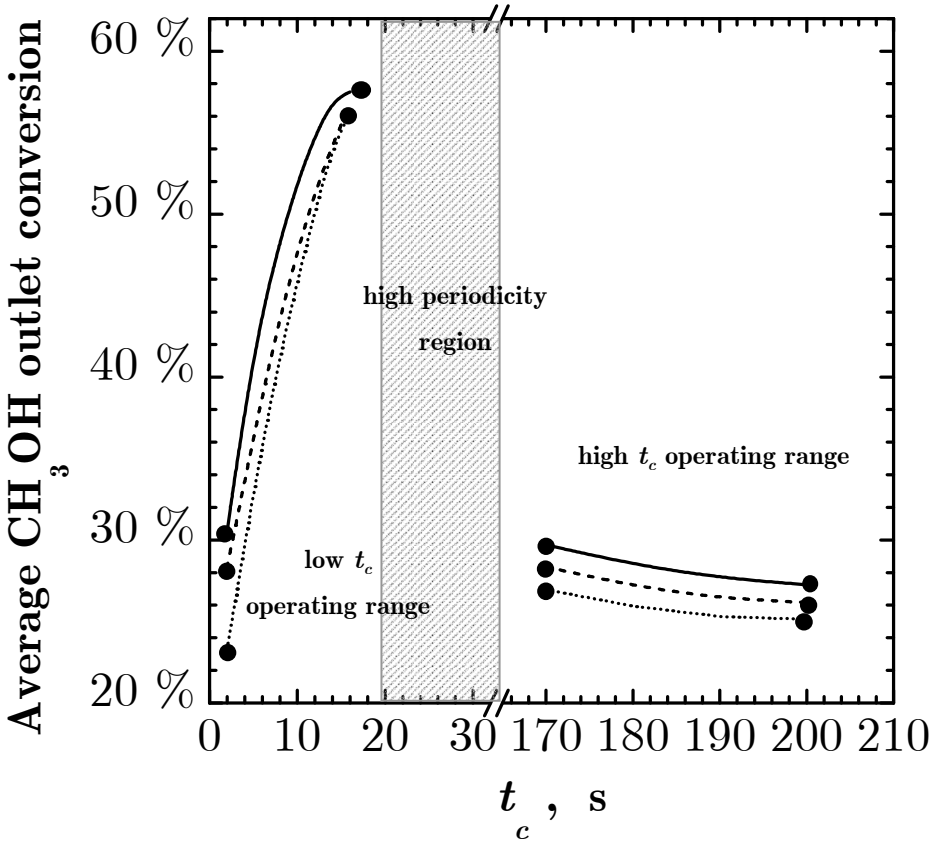
Average CH_3OH outlet conversion
60 %
50 %
40 %
30 %
20 %
high periodicity
region
high t_c operating range
low t_c
operating range
0
10
20
30
170
180
190
200
210
t_c , s

Figure 3

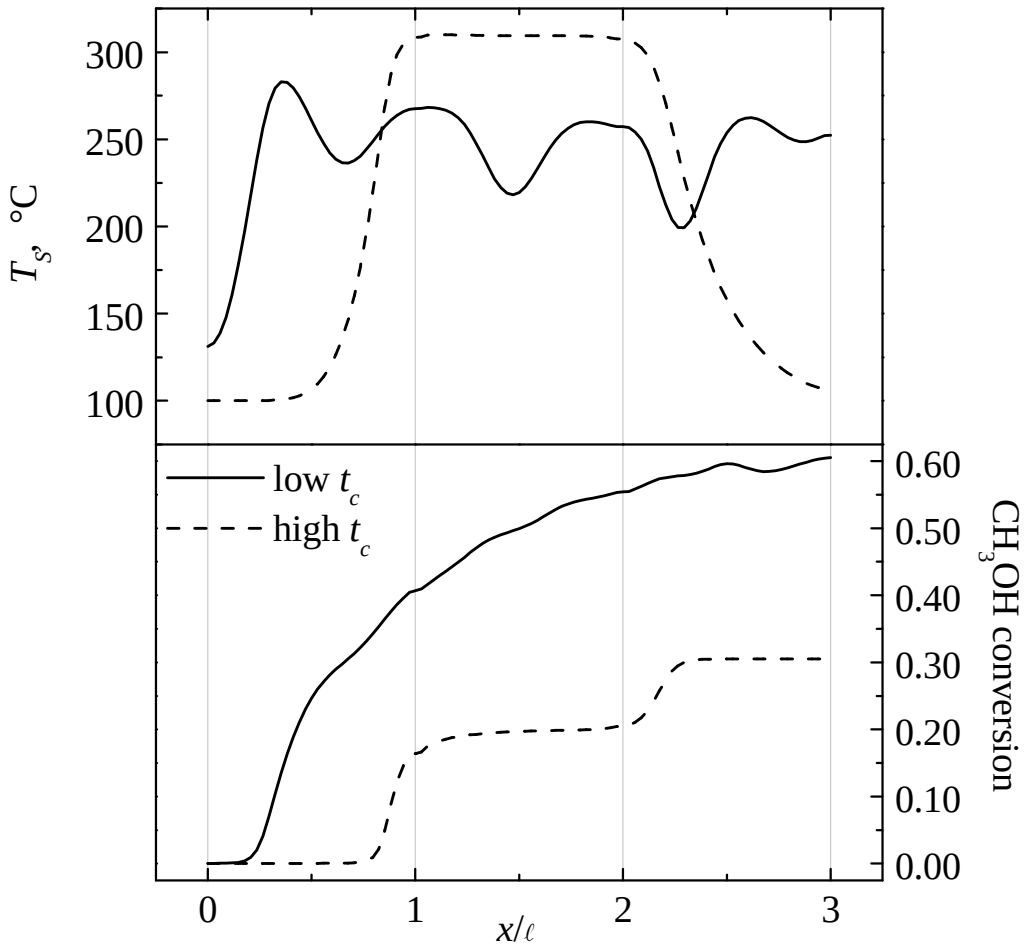
300
250
200
150
100
T_S, °C
low t_c
high t_c
0.60
0.50
0.40
0.30
0.20
0.10
0.00
CH_3OH conversion
0
1
2
3
x/ℓ

Figure 4

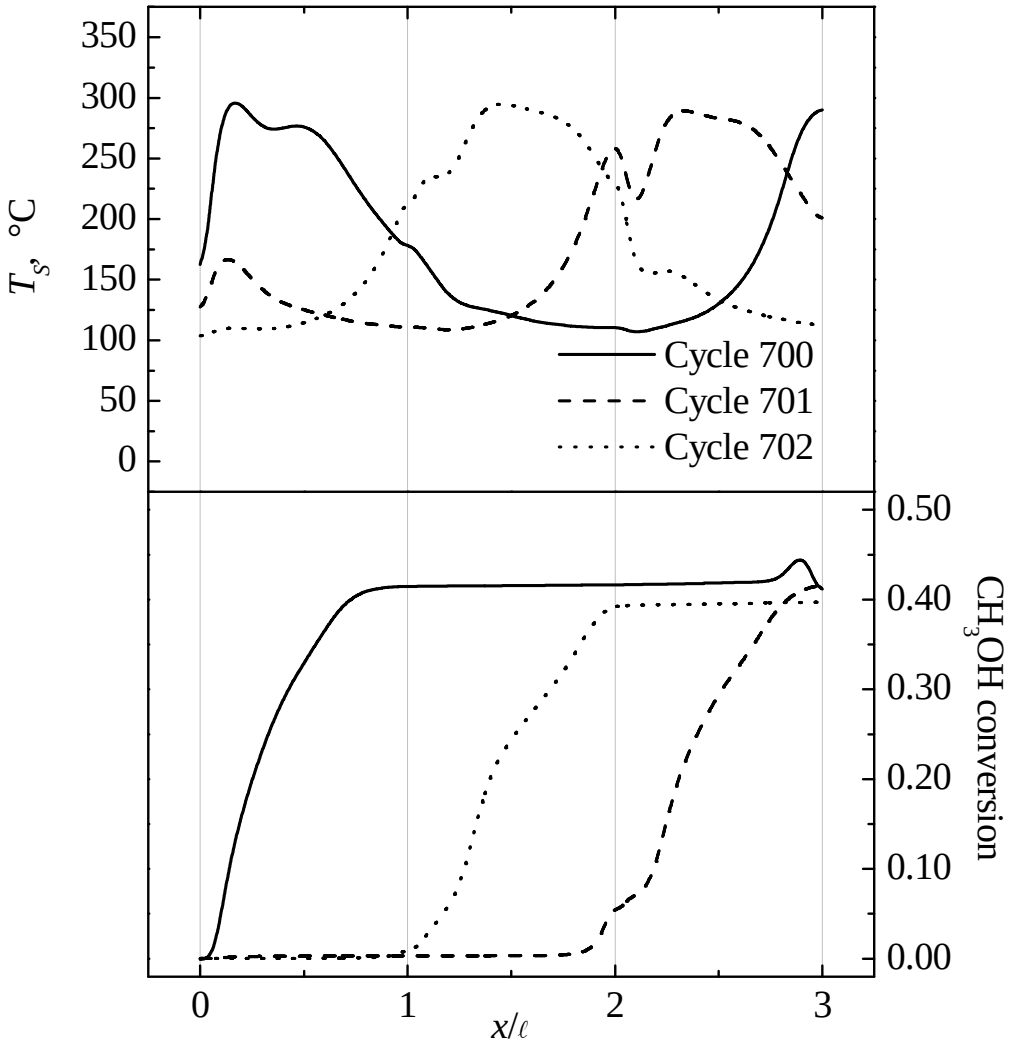
350
300
250
200
150
100
50
0
T_S, °C
Cycle 700
Cycle 701
Cycle 702
0.50
0.40
0.30
0.20
0.10
0.00
CH_3OH conversion
0
1
2
3
x/ℓ

Figure 5

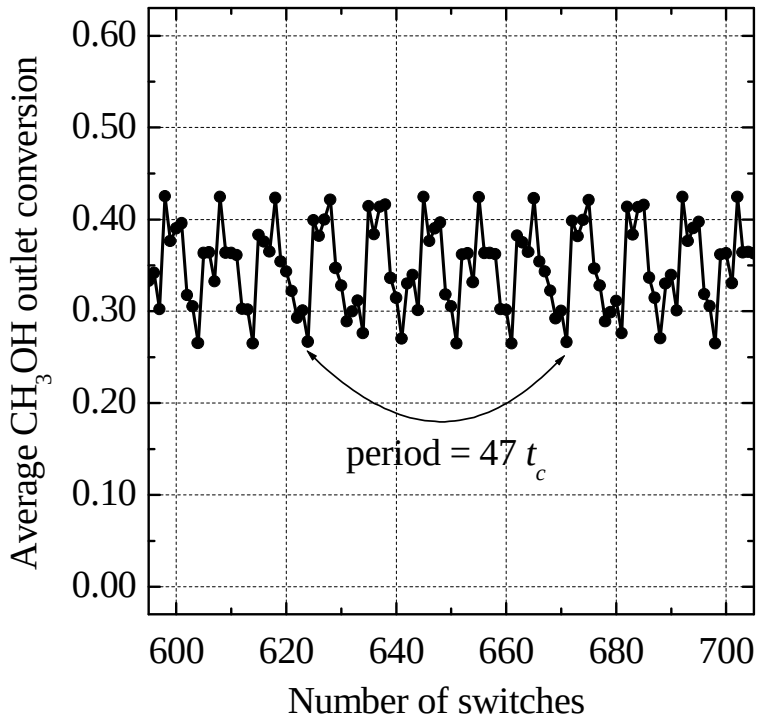
Average CH_3OH outlet conversion
0.60
0.50
0.40
0.30
0.20
0.10
0.00
600
620
640
660
680
700
Number of switches
period = 47 t_c

Figure 6

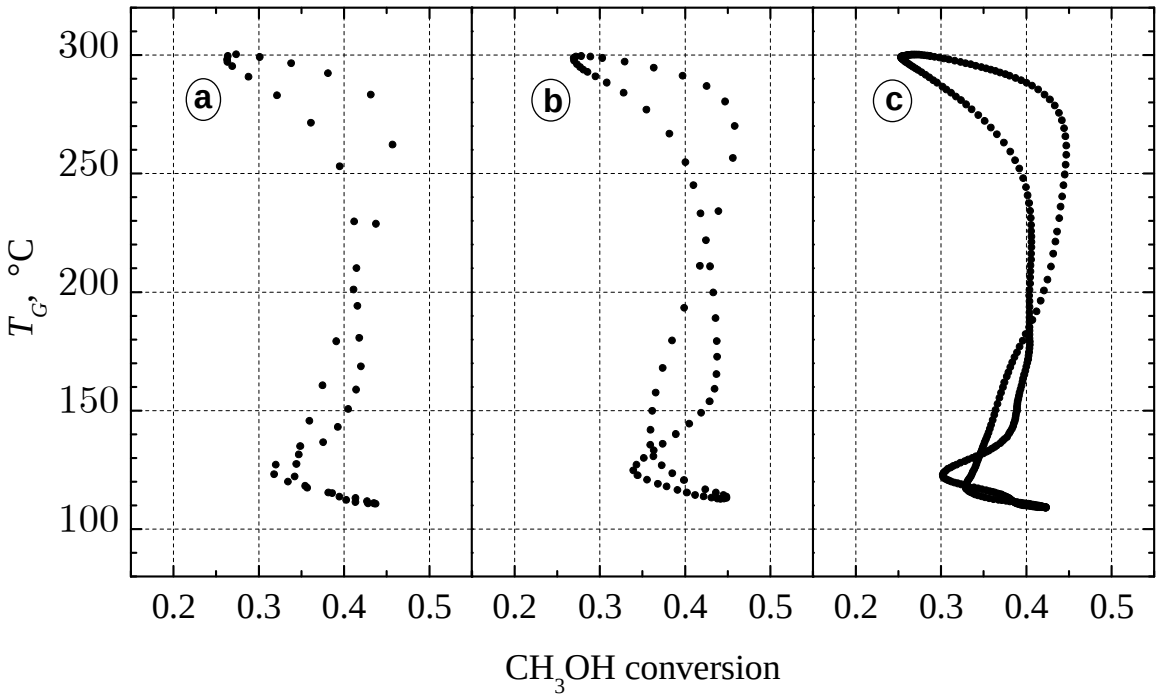

Figure 7

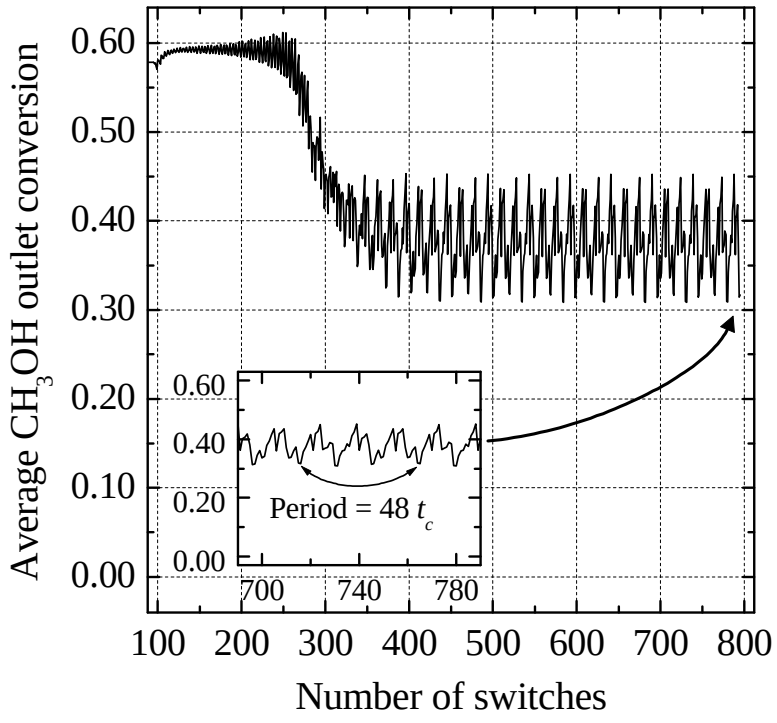
Average CH_3OH outlet conversion
0.60
0.50
0.40
0.30
0.20
0.10
0.00
100
200
300
400
500
600
700
800
Number of switches
0.60
0.40
0.20
0.00
700
740
780
Period = 48 t_c

Figure 8

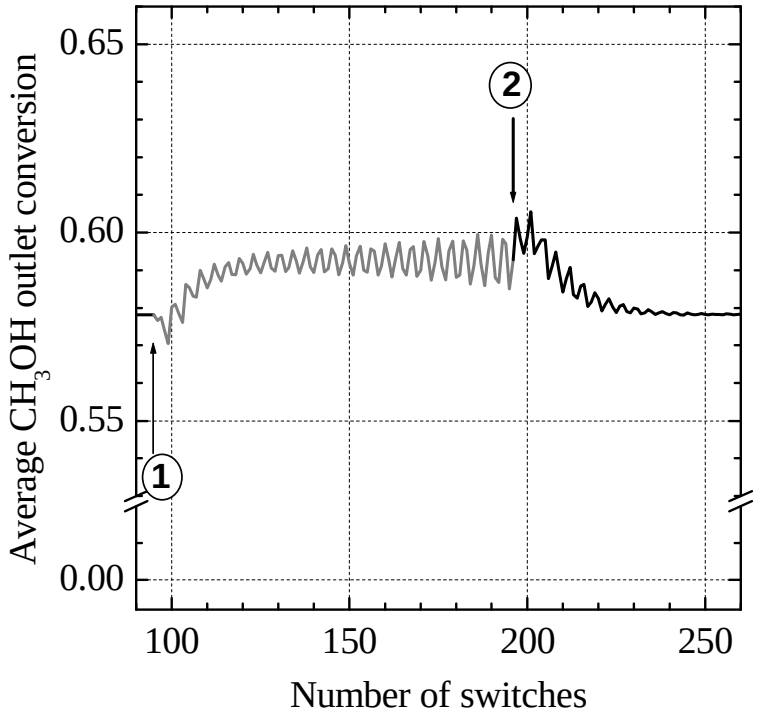
Average CH3OH outlet conversion
0.65
0.60
0.55
0.00
100
150
200
250
Number of switches
1
2

Figure 9

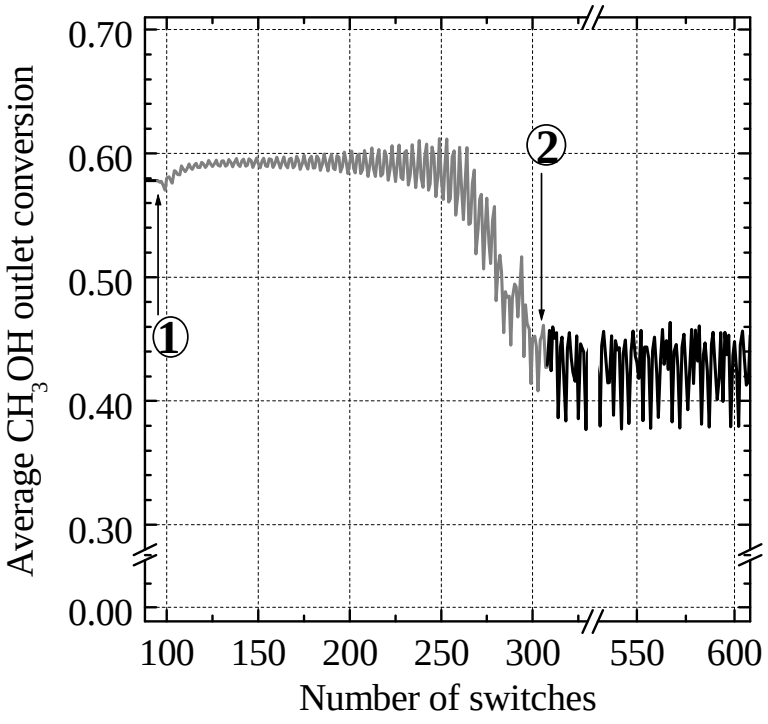
Average CH3OH outlet conversion
0.70
0.60
0.50
0.40
0.30
0.00
100
150
200
250
300
550
600
Number of switches
1
2